Science of the Total Environment 573 (2016) 690–698

Contents lists available at ScienceDirect

Science of the Total Environment

journal homepage: www.elsevier.com/locate/scitotenv

Combined effects of organic aerosol loading and fog processing on organic aerosols oxidation, composition, and evolution

Abhishek Chakraborty [a], Tarun Gupta [a,b,*], S.N. Tripathi [a,b,*]

[a] Department of Civil Engineering, Indian Institute of Technology, Kanpur, India
[b] Centre of Environmental Science and Engineering, CESE, IIT, Kanpur, India

GRAPHICAL ABSTRACT

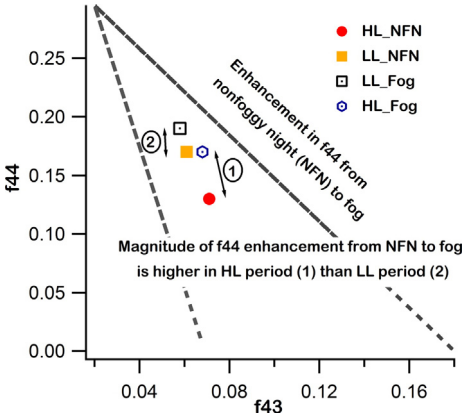

ARTICLE INFO

Article history:
Received 14 May 2016
Received in revised form 29 July 2016
Accepted 22 August 2016
Available online xxxx

Editor: D. Barcelo

Keywords:
Organic aerosols
Loading
Fog
O/C ratio
Aqueous processing

ABSTRACT

Chemical characterization of ambient non-refractory submicron aerosols (NR-PM_1) was carried out in real time at Kanpur, India. The measurements were performed during the winter (December 2014 to February 2015), and comprised of two very distinct high and low aerosol loading periods coupled with prevalent foggy conditions. The average non-refractory submicron aerosol loading varied significantly from high (HL, ~240 μg/m^3) to low loading (LL, ~100 μg/m^3) period and was dominated by organic aerosols (OA) which contributed more than half (~60%) of the measured aerosol mass. OA source apportionment via positive matrix factorization (PMF) showed drastic changes in the composition of OA from HL to LL period. Overall, O/C (oxygen to carbon) ratios also varied significantly from HL (=0.59) to LL (=0.69) period. Fog episodes (n = 17) studied here seem to be reducing the magnitude of the negative impact of OA loading on O/C ratio (OA loading and O/C ratio are anti-correlated, as higher OA loading allows gas to particle partitioning of relatively less oxidized organics) by 60% via aqueous processing. This study provided new insights into the combined effects of OA loading and fog aqueous processing on the evolution of ambient organic aerosols (OA) for the first time.

* Corresponding authors at: Department of Civil Engineering, Indian Institute of Technology, Kanpur, India.
E-mail addresses: tarun@iitk.ac.in (T. Gupta), snt@iitk.ac.in (S.N. Tripathi).

http://dx.doi.org/10.1016/j.scitotenv.2016.08.156
0048-9697/

1. Introduction

Submicron ambient aerosols have an impact on radiative climate forcing and can adversely affect human health (Jacobson et al., 2000; Seinfeld and Pankow, 2003; Jimenez et al., 2009). Most Indian cities suffer from poor air quality, and numerous studies have reported very high pollution levels in all the major cities of India (Venkataraman et al., 2002; Gurjar et al., 2004; Gupta et al., 2006; Sarkar et al., 2010; Joseph et al., 2012). Kanpur, being a major industrial hub and having a population of 4.5 million also suffers from serious air pollution (National Ambient Air Quality Standards, 2012). Numerous offline, 4–8 h long filter based field studies (Kaul et al., 2011, 2012; Ram and Sarin, 2011; Gupta and Mandariya, 2013; Singh et al., 2014) reported very high PM_1 loadings ranging between 100 and 200 μg/m^3 in Kanpur, especially during winter. Although useful; these studies were unable to capture organic aerosol (OA) evolution (gradual changes in nature and properties of OA via aging, volatilization and mixing with a different type of OA (Heald et al., 2010)), which usually occurs over shorter time scales. Advancement in mass spectrometry technique and the arrival of Aerodyne aerosol mass spectrometer (AMS) (DeCarlo et al., 2006; Canagaratna et al., 2007) has provided some in depth information about the real time evolution of OA (Hallquist et al., 2009; Heald et al., 2010). Around the globe, many fields and laboratory studies have been performed using AMS; however, online/AMS based studies have rarely been conducted in the South Asia, world's most populous region. So, very limited information is available about OA evolution and properties from this region (Bhattu and Tripathi, 2015). Thus, the goal of this study was to explore the impact of different parameters like organic aerosol (OA) loading and fog on the real-time evolution of aerosol composition and oxidation (O/C ratio) ratios.

O/C ratio of SOA or OOA (Secondary or Oxidized organic aerosol) is usually negatively correlated with OA loading as reported by a few chamber (Kang et al., 2011; Pfaffenberger et al., 2013) and ambient studies (Ng et al., 2011a; Bhattu and Tripathi, 2015). Higher OA concentration promotes more gas to particle conversion of less oxidized, semi volatile organics (Kang et al., 2011; Ng et al., 2011a). A laboratory (Kang et al., 2011) study has also indicated that the slope of this anti-correlation between O/C ratio, and OA loading depends on aerosol loading regime. However, such dependence has not yet been reported from field studies and the causality for this observation has not been explored in either laboratory or field studies. Observed high and low OA loading conditions in this current study provided a unique opportunity to explore this OA loading-dependent SOA oxidation under ambient conditions. During winter of every year, Kanpur is affected by several fog episodes of short (3 h) to long durations (17 h) that severely hampered regular activities of local people. Fog episodes can also contribute to the formation of secondary organic aerosols (SOA) via aqueous phase oxidation, as reported in several previous field and lab studies (Dall'Osto et al., 2009; Kaul et al., 2011; Ge et al., 2012; Li et al., 2013; Chakraborty et al., 2015).

A previous filter based study at the same location reported 60% enhancement OC/EC ratio during fog events (Kaul et al., 2011) compared to non-foggy period. Online AMS based studies carried out in Fresno, California and Hong Kong, (Ge et al., 2012; Li et al., 2013) observed slightly enhanced O/C ratio and f44 (= m/z 44/total OA). In AMS, m/z 44 or CO_2^+ fragment is considered to be a marker for carboxylic acid moieties (Takegawa et al., 2006a) and f44 represents the fractional contribution of m/z 44. Enhanced f44 levels during fog and haze events indicate the formation of more aged/oxidized of OA, highlighting the impact of aqueous processing of the submicron aerosols. Lee et al. (2012) performed laboratory oxidation of cloud water samples and particulate organics collected at a mountain site. They reported significant enhancement in organic mass, f44, and O/C ratio due to functionalization for cloud water samples. However, as oxidation progresses these enhancements slowed down possibly due to the dominance of fragmentation. On the contrary, they found that organic aerosols extracted from the filters became more volatile and lost organic mass due to the dominance of fragmentation from the very beginning of the oxidation process. During 2012–13 winter, enhancement in f44, O/C ratio and OOA contribution during fog events has already been reported at this location from an AMS based study (Chakraborty et al., 2015). Collett et al. (2002, 2008) reported high concentrations of dicarboxylic acids in fog water from different places of US. They also reported preferential scavenging of more oxidized wood burning aerosols than less oxidized vehicular exhaust. Gilardoni et al. (2014) from a study in Po Valley also reported a good correlation between organic aerosol scavenging and O/C ratio. So, the impact of cloud/fog processing on OA oxidation has been reported around the globe with considerable details. However, combined effects of two parameters; OA loading and aqueous oxidation with different impacts on OA oxidation level (O/C ratio) have never been studied anywhere. OA loading decreases O/C ratio as mentioned earlier, however, aqueous oxidation/processing can enhance the OA oxidation level and depends more on aerosol/fog/cloud liquid water content (LWC) rather than OA loading (Volkamer et al., 2009; Ervens et al., 2011). Therefore, it would be interesting to examine the combined effects of OA loading and fog/aqueous processing on existing OA composition and oxidation at this polluted location.

2. Materials and methods

2.1. Site of study and measurement period

Measurements were performed in the campus of Indian Institute of Technology (IIT) Kanpur (26.46°N, 80.33°E, and 142 m above sea level) from 18 Dec 2014–10 February 2015. Kanpur is a large city of ≈4.5 million (GOI, 2011) population and located in the center of the Gangetic Plain (GP), but having very poor air quality (National Ambient Air Quality Standards, 2012). IIT Kanpur is located upwind of the city center and within the city boundaries. Based on NR-PM_1 (non-refractory submicron aerosols; part of the submicron aerosols that evaporates within few seconds at 600 °C (Zhang et al., 2005c)) loading, the entire campaign was divided into two separate periods. The 1st period (termed as high loading, HL) was from 18 Dec 2014–01 Jan 2015 with an average NR-PM_1 loading of 239 (±73) μg/m^3, and several frequent fog events (10 events in 15 days). The 2nd period (low loading, LL) was from 02 January 2015–10 February 2015 with an average NR-PM_1 loading of 101 (±39) μg/m^3, and several but infrequent fog events (7 events in 40 days), respectively. Meteorological parameters and CO concentrations for both the periods are listed in Table 1.

RH & T values were obtained from Vaisala RH & T sensor (Model: HMT 331), deployed at the same laboratory along with other instruments. Wind speed (DWA 8600, Dynalab Weathertech), precipitation (DTR 8104, Dynalab Weathertech), and solar radiation (CMP 6, Kripp & Zonen) data were obtained from an automated weather station located near vicinity while the PBL heights were obtained from NOAA ARL archive. CO data was obtained from Thermo Fisher CO analyzer (Model: 49i) instrument kept at the rooftop of the laboratory building.

To analyze the effects of fog, we further divided both the HL and LL period into several sub periods like; fog, prefog, non-pre fog, non-foggy night, postfog, non-post fog. Usually, 90% of the total fog hours were confined within 11 pm–8 am time frame, so this period is taken as foggy period. Prefog (PrF) period is considered to be 5 h before the commencement of the fog; 6–11 pm, while postfog (PoF) period is 8 am-6 pm. Identical time periods, taken for non-foggy periods, are termed as non-pre foggy (NPrF, 6–11 pm), non-foggy night (NFN, 11 pm–8 am) and non-post foggy period (NPoF, 8 am–6 pm). Fog can be defined as an atmospheric condition with low visibility (<1 km) and very high RH (close to 100%, WMO, 1996). In absence of visibility measurements, in this study, start of the fog event was marked when LWC (liquid water content) ≥80 mg/m^3 for ≥15 min (Gilardoni et al., 2014) and end of the fog event was marked when LWC < 80 mg/m^3 for >15 min (Fig. S1).

Table 1
Average (±1 std) values for different meteorological and emission parameters during HL and LL period. PBL = planetary boundary layer, WS = wind speed, SR = solar radiation, CO = carbon monoxide.

Parameters	HL			LL		
	Non-fog		Fog	Non-fog		Fog
	Day	Night		Day	Night	
RH (%)	74.3 ± 8.2	87.4 ± 5.1	96.9 ± 2.9	73.8 ± 6.9	86.8 ± 6.8	95.8 ± 3.5
T (°C)	12.9 ± 3.8	9.8 ± 2.6	7.2 ± 2.1	14.2 ± 3.9	11.1 ± 2.2	7.5 ± 1.9
PBL (m)	492 ± 80	100 ± 28	101 ± 22	550 ± 92	141 ± 30	102 ± 25
WS (m/s)	2.9 ± 0.9	2.7 ± 0.8	1.9 ± 0.5	2.7 ± 1	2.6 ± 0.4	1.8 ± 0.6
CO (ppm)	1.2 ± 0.2	1.3 ± 0.3	1.3 ± 0.2	1.1 ± 0.3	1.1 ± 0.4	1.2 ± 0.2
SR (W/m^2)	351 ± 100			231 ± 60		
Rainfall (mm)	0			15 ± 5	11 ± 4	

2.2. Instrumentation

An HR-ToF-AMS (high-resolution time-of-flight aerosol mass spectrometer) (DeCarlo et al., 2006; Canagaratna et al., 2007) was used along with other collocated instruments; scanning mobility particle sizer (SMPS, Model 3696, TSI Inc.), CO analyzer (Thermo Fisher scientific, USA, Model 49i), cloud combination probe (CCP, DMT, to measure the LWC) and E-BAM (Environment Proof-Beta Attenuation Monitor, Met One Instruments, USA) for measuring $PM_{2.5}$ mass concentration at every 15 min interval. A home built thermodenuder (TD) was also placed in front AMS to characterize aerosol volatility, and an automated switching system enabled ambient air to pass through TD to AMS and directly to AMS at every 10 min interval. TD was built in-house with a 1 m heating section (hollow metal tubes with 1 cm internal diameter with heating coils wrapped around it) followed by a 1 m long charcoal denuder section to prevent re-condensation of volatilized material. In this manuscript, however, we will only be discussing ambient aerosol characterization. Also, a silica gel drier was placed in front of the AMS to stop direct entry of moisture. Aerosol transmission efficiency of aerodynamic lenses inside the AMS is 100% for 60–700 nm size range (Liu et al., 2007), and decreases rapidly after that, so in a strict sense, AMS doesn't have a well-defined PM_1 cut point. However, in most published literature including the initial ones on AMS characterization, aerosols sampled by AMS termed as "NR-PM_1 (non-refractory submicron aerosol)" or simply as submicron aerosols, so we have used NR-PM_1 throughout the paper.

Typical fog droplet size is much higher than 1 μm so in the case of a fog event AMS can only characterize interstitial aerosols, submicron unactivated wet aerosols (Frank et al., 1998; Gultepe et al., 2007) and aerosol residues left behind after fog evaporation (Eck et al., 2012; Li et al., 2014). Since these fog processed residues and unactivated wet aerosols will mostly be absent during non-foggy periods, so AMS can still provide valuable insights into the impact of fog processing on OA via comparison with non- foggy periods. The AMS was operated in high sensitivity V mode with a 2 min sampling time; W mode was discontinued after few days due to very frequent hard mirror voltage issues which rendered W mode data unusable. Regular IE calibrations were performed to detect any fluctuations of AMS performance. Apart from that, HEPA (High efficiency particulate arrestance, Whatman) filtered ambient air measurements were taken at every alternate day and during IE calibrations to quantify the gaseous interference in the mass spectra.

The CCP (Droplet measurement technology Inc., USA) was placed on the roof of the laboratory building (10 m above the ground) where other instruments were housed. The CCP designed for aircraft sampling and can measure different cloud related parameters. However, in this study, the inlet was modified using an aspirator (Singh et al., 2011) to make it suitable for ground level sampling and only the CDP (cloud droplet probe) part was used to measure fog LWC and droplet size distributions (from 3 to 50 μm) (Lance et al., 2010).

2.3. Data analysis

The AMS unit-mass-resolution (UMR) and high-resolution (HR) data were analyzed in IgorPro, using the data analysis toolkit SQUIRREL (v1.51H) and PIKA (v1.10H), respectively. HR fitting of the HR dataset was carried out till m/z 150. Data-processing procedures are thoroughly described in the previously published literature (Allan, 2003; Aiken et al., 2007, 2008). PMF analysis was carried out on HR OA spectra via PMF evaluation tool (PET) (Paatero and Tapper, 1994; Ulbrich et al., 2009). The accuracy of the reported AMS mass concentration is influenced by the choice of the CE (collection efficiency) value, a factor used to compensate for the aerosol particles lost during transmission through aerodynamic lenses and/or bounces off vaporizer surface without getting ionized (Docherty et al., 2013). Most of the field studies report CE = 0.5 to be good enough to obtain quantitative agreement with other collocated instruments (Canagaratna et al., 2007; Docherty et al., 2013). In this study also, the similar value is found for both the periods using Middlebrook et al. (2012) formulation, which considers the influence of particle acidity, the chemical composition of aerosols and inlet RH on CE value. Use of this CE value (0.5) is also justified by good correlation of AMS vs E-BAM mass concentrations (slope = 0.66, R^2 = 0.73, Fig. S2). AMS NR-PM_1/E-BAM $PM_{2.5}$ ratio (= 0.66) from this study matches well to that of a previously reported $PM_1/PM_{2.5}$ value (~ 0.70) at this location (Kumar et al., 2014). Other uncertainties related to AMS measurements are described in the previously published literature (Allan, 2003; Aiken et al., 2007; Bahreini et al., 2009). Modification of standard AMS fragmentation table was done at m/z values of 15, 29, and 44, based on HEPA/zero filtered measurements.

A back trajectory (BT) analysis was performed for both the HL and LL periods by the hybrid single-particle Lagrangian integrated trajectory (HYSPLIT4) model developed by NOAA/ARL (Draxler and Rolph, 2003). Meteorological data required for the trajectory computations were obtained from the Global Data Assimilation System (GDAS) archive of ARL (available online at http://ready.arl.noaa.gov/archives.php). First, calculation BTs with 48 h duration and starting at 500 m above the ground in Kanpur (26.46°N, 80.33°E) were recorded at every 6 h throughout the loading periods. Next, clustering of the calculated trajectories was performed using HYSPLIT4 software based on similarities in spatial distributions of computed BTs. The principles and processes behind this clustering method can be found in the software user guide (Draxler et al., 2014). The 6-cluster (1 to 6) solution was found to be optimum, and the mean BTs of each cluster are shown in Fig. S3.

3. Results and discussions

3.1. Source apportionment of OA via PMF (positive matrix factorization)

The entire campaign is divided into high and low loading period based on NR-PM_1 loading as mentioned earlier. Detailed description about overall NR-PM_1 loading, composition, and contributions from different back trajectories for both the periods can be found in Supplementary Section 1 (Fig. S4). Ambient OA source apportionment via PMF revealed 3 oxidized OA (OOA) factors along with 4 primary OAs. Oxidized OA factors (OOA-1,2 and O-BBOA) are identified based on their higher O/C ratio and dominance of m/z 43,44 signals in their respective mass spectra (Zhang et al., 2005b; Ng et al., 2011a). OOA-1,2 can also be termed as SV (semi volatile) LV (low volatile) OOA, as OOA-2 has higher O/C ratio (= 1.19) than OOA-1 (= 0.96) and higher O/C ratio is generally associated with less volatile OA (Jimenez et al., 2009; Ng et al., 2011a). However, in the absence of dedicated volatility measurement

of individual OA factors we choose to name them OOA-1,2; which are also very common terms and used widely in published literature (Bhattu and Tripathi, 2015; Chakraborty et al., 2016b). Apart from higher O/C ratio, OOA-2 has a much higher f44/f43 ratio (=8.42) than OOA-1 (=4.35) (f43 = m/z43/total OA). In AMS, m/z 43 or $C_2H_3O^+$ fragment is a marker for less oxidized aldehyde or ketone moieties (Takegawa et al., 2006b), and f43 is the fractional contribution of m/z 43 to total OA. Increasing f43 indicates the formation of freshly oxidized and moderately volatile organics. The higher f44/f43 ratio of OOA-2 shows that has more organic acids moieties and most likely less volatile than OOA-1 (Ng et al., 2011a). Biomass burning OAs are identified based on the presence of a substantial signal at m/z 60 ($C_2H_4O_2^+$ fragment, a tracer fragment that originates from levoglucosan, which is an integral part of any biomass cellulose) (Cubison et al., 2011). BBOA factors 4, 6 and 7 have relatively lower O/C ratios and well within the range of primary BBOAs as mentioned in several previous studies (Aiken et al., 2010; Cubison et al., 2011), so they are considered as primary BBOAs. However, some differences exist among them as well. Factor 4 (BBOA-1) has highest amount of CHN fragments and N/C ratio among all other primary BBOAs [factor 6 (BBOA-2) and factor 7 (BBOA-3)]. Factor-6 (BBOA-2) has highest O/C ratio and lowest signals at higher m/z's (>100) among all other primary BBOAs (Fig. 1). Factor 3 has a good signal at m/z 60 and m/z 44 (a tracer for highly oxidized organic acids) along with a much higher O/C ratio than primary BBOAs (they typically have 0.2–0.4 O/C ratio (Aiken et al., 2010)), so it is termed as oxidized BBOA (O-BBOA). Primary BBOAs have strong m/z 60 signals but very low m/z 44 levels and O/C ratios. Depending upon types of biomass burned and the temperature of burning, mass spectra of BBOA vary greatly (Saarikoski et al., 2008; Ortega et al., 2013), so identification of various types of BBOA is not surprising. Previous studies have also identified various types of BBOA in this location and elsewhere (Timonen et al., 2013; Bhattu and Tripathi, 2015; Chakraborty et al., 2015; Lee et al., 2015). HOA (hydrocarbon like OA) is generally identified by dominance of CH fragments in their mass spectra with very low m/z 43, 44 signals and O/C ratio. HOA generally originates from primary sources like vehicular exhaust and has similar properties like EC (elemental carbon) (Zhang et al., 2005a). Similar types of OA factors were also identified in 2012–13 winter via AMS–PMF. However, 2012–13 winter study was relatively short (for 3 weeks, 20 December–10 January) and aerosol loading was fairly similar throughout that foggy period, so the impact of OA loading on OA composition and evolution could not be studied (Chakraborty et al., 2015). On the contrary, in this study two very distinct ambient OA loading period was observed. For PMF diagnostics, the rationale behind choice of factors, comparison with external tracers and OA diurnal variation, please refer to SI (Sections 2.1 & 2.2, Table S2 and Fig. S5–S7).

3.2. OA loading impact on OA composition and characteristics

During HL period, overall OA mass concentration and O/C were 134 ± 42 μg/m^3 and 0.59 ± 0.09, respectively. While during LL period overall OA mass concentration and O/C were 56 ± 20 μg/m^3 and 0.69 ± 0.1, respectively (differences in OA mass concentrations and O/C ratio between two loading periods are very statistically significant, $p < 0.0001$). These differences in mass concentrations were most likely caused by lower combustion pollutant influence as indicated by lower CO values during LL period combined with higher daytime boundary layer heights and scavenging by sporadic light rainfall (Table 1). Diurnal O/C ratio (Fig. 2) for HL and LL revealed a persistent difference in O/C ratio throughout the day which peaked during daytime most likely due to intense photochemical oxidation of OA. H/C ratio peaked at morning and evening traffic rush hours due to enhanced vehicular emissions (mostly HOA). H/C ratio reached its lowest diurnal value during afternoon hours due to the reduction in primary emission and ongoing photochemical oxidation of OA.

O/C ratio decreases with increasing OA loading in both the loading period, however, the rate of decline was much steeper during LL than HL (Fig. 3). A similar kind of observation was reported by Kang et al. (2011) in a lab study during oxidation of α – pinene via OH radicals. However, the negative correlation between O/C ratio and OA loading has rarely been reported from ambient studies (Ng et al., 2011a).

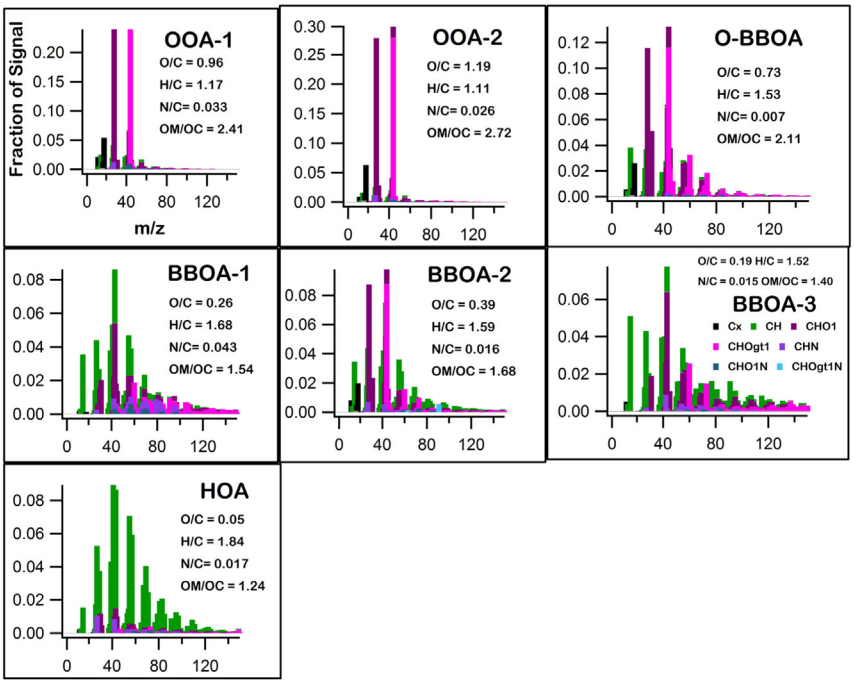

Fig. 1. Different types of OA, as identified by applying PMF on HR AMS organic mass spectra. X axis indicates mass to charge ratio (m/z) while Y axis represents normalized fractional contribution of each m/z to the total signal (=1) of that particular factor.

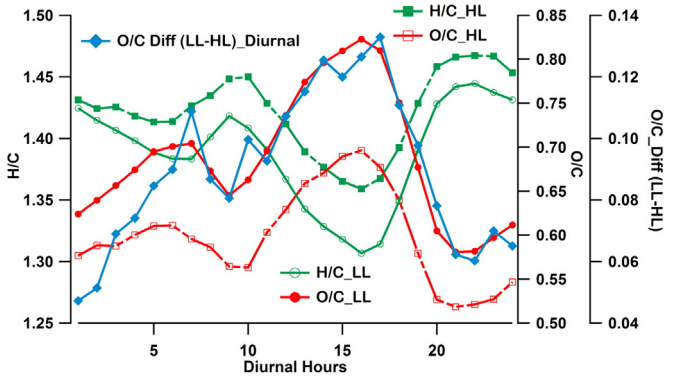

Fig. 2. Diurnal pattern of different elemental ratios. Afternoon peak in O/C and subsequent decrease in H/C indicate photochemical oxidation and reduction in primary emissions. Late night/early morning peak in O/C ratio possibly indicates enhanced aqueous and gas phase chemistry due to stagnant conditions and presence of fog. O/C_Diff (LL-HL) shows the difference between LL and HL period O/C ratio at different diurnal hours.

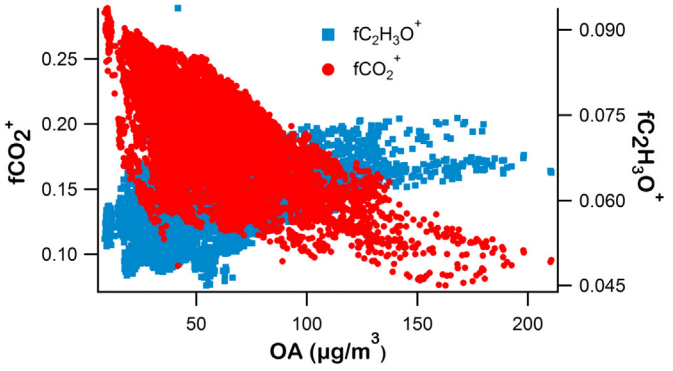

Fig. 4. OA loading dependency of more (CO_2^+) and less ($C_2H_3O^+$) oxidized OA fragments. Left and right side x-axis represents fractional contributions of CO_2^+ (originates from fragmentation of carboxylic acids) and $C_2H_3O^+$ (originates from fragmentation of aldehydes/ketones in AMS) fragments to total OA in the AMS.

During high OA loading, gas to particle conversion of less oxidized organics is favored, leading to a lower O/C ratio (Kang et al., 2011; Ng et al., 2011a). In this study also with increasing OA loading, fractional contribution of $C_2H_3O^+$ (which often considered as a marker for less oxidized freshly produced SOA) increases, while that of CO_2^+ (a marker for highly oxidized organic acids) (Takegawa et al., 2006b; Chakraborty et al., 2015) decreases (Fig. 4). So, these observations support the hypothesis that partitioning of less oxidized organics from gas to particle phase is favored under HL condition.

However, higher contributions from POA with increasing OA loading (Fig. S8) may have also contributed to this observed anti-correlation between OA loading and O/C. Increased loading of POAs (especially of BBOA) during highly polluted haze-fog episodes was also reported from a study conducted in Yangtze river delta in China (Zhang et al., 2015). Apart from that f44/f43 ratio was also higher during LL period (=3.12) than in HL period (=2.18). This ratio (f44/f43) has been linked to aerosol volatility in previous studies (Kang et al., 2011; Ng et al., 2011a) implying that during LL period non-volatile organics contributed more towards total OA. Although overall NR-PM_1 composition varied little from HL to LL, PMF results revealed that the type of dominant OOA changed drastically from HL to LL. The contribution of the most oxidized factor OOA-2 (O/C = 1.19) increased almost 5–10 folds from HL to LL while that of OOA-1 decreased by the same order (Fig. 5). LL possibly favored gas to particle partitioning of this highly oxidized OOA-2 compared to less oxidized OOA-1 resulting in such a drastic change. LL also favored gas to particle partitioning of less volatile organics as partitioning coefficient saturation vapor pressure is inversely proportional to the mass loading (Pankow, 1994; Kroll and Seinfeld, 2008). The higher f44/f43 ratio of OOA-2 (=8.42) compared to OOA-1 (=4.35) indicates that it is less volatile among two OOA factors and thus more favorably partitioned to particle phase under LL condition than OOA-1. It is also possible that some differences are caused by the different types and/or magnitude of particle phase reactions during different loading periods.

Besides having higher O/C ratio than OOA-1, OOA-2 also has a higher f44/f43 ratio (Fig. S9) which has been shown to be anti-correlated with OA volatility (Kang et al., 2011). This indicates that most likely OOA-2 is less volatile than OOA-1. This steeper decrease of O/C ratio during LL can be explained by the rapid decline of the most oxidized OOA-2 (O/C = 1.19) with increasing OA loading (Fig. S8). Fig. S8 also revealed that under both loading conditions, enhancement in OA loading was mostly due to primary BBOAs.

3.3. Combined influence of fog on OA composition and evolution under different loading conditions

During the entire study period, several fog events (=17) were observed. As mentioned earlier, fog events were much more frequent during HL period (on average one fog event in every 1.5 days) than LL period (on average one fog event in every 6 days), in spite of very similar meteorological parameters (Table 1). This suggests a possible link

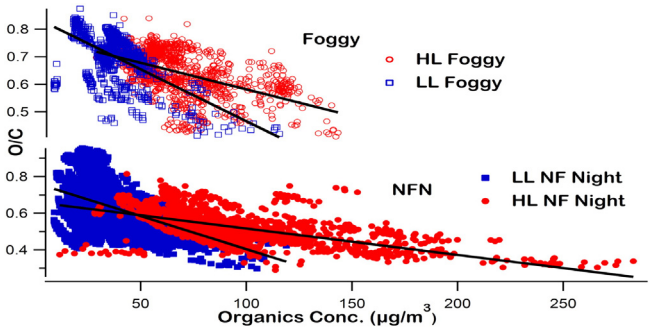

Fig. 3. OA loading dependent change in O/C ratio. Different rates (rate difference is statistically very significant, $p < 0.0001$) of O/C decrease for different OA loading periods.

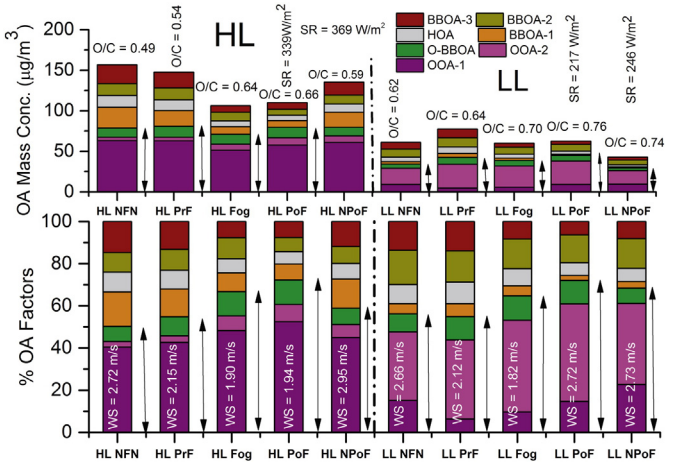

Fig. 5. OA composition dependency on OA loading. SR = solar radiation (W/m^2), WS = wind speed (m/s). Arrows indicate total OOA concentrations and contributions. Most dominant OOA type has changed from OOA-1 to OOA-2 with a decrease in OA loading. Black dotted line divides HL and LL period. During the foggy period under both the loading conditions, total OA mass decreases due to fog scavenging but the relative contribution of OOAs and O/C ratio increases. This indicate that the production of OOAs inside the fog is somewhat subduing its role as a scavenger.

between air pollution and frequency of fog formation as mentioned in some of the previous studies (Kokkola et al., 2003; Vautard et al., 2009; Quan et al., 2011; Syed et al., 2012). As mentioned earlier AMS can't sample fog droplets directly due to their larger sizes, but AMS can detect fog processed residues that are left behind after fog evaporation in the sub-micron range particles (Ervens et al., 2011; Eck et al., 2012; Li et al., 2014). Also, fog (especially polluted fog) contains a large number of unactivated wet aerosols (Frank et al., 1998; Gultepe et al., 2007; Elias et al., 2009), which may have also undergone some aqueous processing. In the absence of these fog processed residues during non-foggy periods, a comparison of foggy and non-foggy periods can reveal the impact of fog (aqueous processing) on the OA evolution. It has been observed in this study that fog can alter OA composition and evolution effectively though with varying magnitude in both HL and LL conditions. Fig. 6a is showing a comparison between foggy vs. non-foggy night for HL and LL conditions. Interestingly, f44 level during HL foggy period (OA loading = 110 ± 35 μg/m^3) was similar to that of LL non-foggy night (OA loading = 60 ± 16 μg/m^3), in spite of much higher OA loading during the HL fog (Fig. 5). This cannot be explained solely by gas phase oxidation and subsequent gas to particle conversion since both f44, and O/C ratio are usually anti-correlated with OA loading (Kang et al., 2011; Ng et al., 2011b). This is likely due to enhanced contributions from OOAs during fog, which is known to produce highly oxidized products (like organic acids) (Ervens et al., 2004, 2011; Carlton et al., 2007; McNeill, 2015) via aqueous processing. Night time fog/aqueous oxidation can be driven by dark Fenton reactions, where transition metals (Fe, Cu) produce OH radicals in fog droplets, fog/cloud droplets can also scavenge gas phase OH radicals from atmosphere as demonstrated from this location and elsewhere (Yasmeen et al., 2010; Ervens et al., 2014; Al-Abadleh, 2015; Chakraborty et al., 2016a). Also, NO_3 radicals and O_3 (Brown et al., 2009) can act as oxidizing agents as well. So, plenty of drivers are available to drive night time oxidation reactions.

Aqueous processing influenced more by liquid water content and solute concentration than OA loading (Ervens et al., 2003, 2011; Volkamer et al., 2009), so during HL fog, it reduced the negative impact of higher OA loading on f44, resulting in similarly high f44 level as LL non-foggy night. Similar upward left movement during aqueous oxidation of cloud water organics has been observed in some laboratory based studies as well (Lee et al., 2011, 2012). The same plot revealed that the difference between LL and HL non-foggy night f44 levels (=0.17 and 0.12, respectively, difference = 0.05) is higher than the same difference during foggy period (=0.19 and 0.17, respectively, difference = 0.02, differences are statistically very significant, $p < 0.001$) indicating that fog processing of OA reduces the magnitude of negative impact of OA loadings on OA oxidation.

It is also very important to evaluate whether some other parameters like meteorology, local emissions, and transported aerosols have contributed significantly to the observed differences between foggy and non-foggy period. Meteorological parameters varied little from HL to LL and from fog to non-foggy period as shown in Table 1. Anthropogenic emissions, as indicated by CO (Carbon monoxide) (Cabada et al., 2004; De Gouw and Jimenez, 2009) concentrations, was also not very different from foggy to non-foggy nights within a loading regime (Table 1). Also, during fog, lower boundary layer height and stagnant condition reduce the impact long range transport, and local processes dominate (Dall'Osto et al., 2009; Chakraborty et al., 2015). Apart from that, fog scavenges oxidized OA more efficiently than less oxygenated POAs (Gilardoni et al., 2014), still O/C and OOA contributions increased, indicating that production of aqSOA inside fog was countering OOA removal. So, it can be said that observed differences from foggy to non-foggy periods were mainly originated from the efficient processing of OA inside the fog droplets, which has already been demonstrated from this location (Chakraborty et al., 2016a). The role of fog in reducing the negative impact of OA loading on OA oxidation is also evident from Fig. S10. In Fig. S10, when non-foggy and foggy period O/C diurnal cycles are plotted separately, it is found that in a non-foggy cycle (non-pre fog to non-foggy night to non-post fog), HL and LL period O/C ratios maintained a constant gap throughout the diurnal hours. However, during a foggy cycle (prefog to fog to postfog), night time O/C ratios from HL and LL period are much closer than a non-foggy cycle while daytime gap remains almost the same. Fog events typically occurred during night time (11 pm–8 am), so, reduced O/C gap during night time indicates that the fog has played a role in this reduction via loading independent aqueous processing (Fig. S10). The enhancement in f44 levels (Fig. 6a) (and O/C ratio, Fig. S10) from non-foggy night to foggy nights is also more pronounced in HL period than LL period. Since background OA during LL period was already more oxidized than that of HL period, so effects of fog processing seemed to be moderate when compared to those during the HL period. It is also possible that infrequent fog events with slightly lower LWC (Fig. S1) during LL may have restricted aqueous oxidation via fog to some extent.

During both foggy and non-foggy periods, from prefog/non-pre foggy to postfog/non-post foggy period, there was a continuous lower-right to top-left movement of OA inside the triangle area (Fig. 6b)

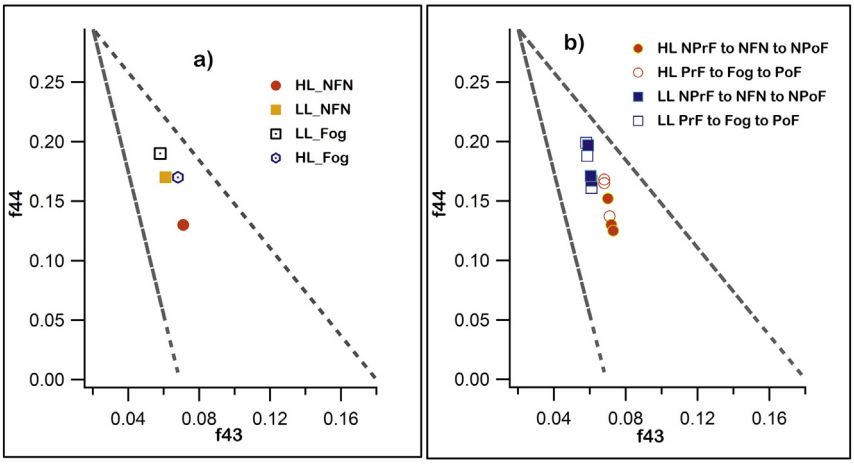

Fig. 6. a) f44 vs. f43 triangle plot of HL and LL period. Dashed lines indicate the region within which most ambient data resides (Ng et al., 2011a). Those periods are further divided into foggy and non-foggy periods. During fog, HL and LL f44 levels were much closer than non-foggy nights. This indicates fog can partially negate the negative OA loading influence on OA oxidation/aging. b) Combined effects of OA loading and fog chemistry on OA evolution. A complete foggy (Prefog, PrF + Fog + Postfog, PoF) and non-foggy cycle (non-pre fog, NPrF + non-foggy night, NFN + non-post fog, NPoF) is plotted here separately for both the loading period. 3 points in each cycle from bottom to top represents pre-fog/non-pre fog (6–11 pm), fog/non-foggy night (11 pm–8 am) and post-fog/non-post fog (8 am–6 pm) for both the loading periods, respectively.

indicating conversion of carbonyls/alcohols moieties (as indicated by f43) to organic acids/peroxides moieties (as indicated by f44). However, nature of this movement differs significantly from non-foggy to foggy periods. During the foggy period, the largest shift in f44 was seen from prefog (6–11 pm) to fog (11 pm–8 am) while for the non-foggy period it was from non-foggy night (11 pm–8 am) to non-post foggy day (8 am–6 pm) transition. This implies that during the non-foggy period, photochemical oxidation during daytime hours (8 am–6 pm) was the primary cause of f44 enhancement whereas for the foggy period, mostly night time (11 pm–8 am) aqueous chemistry played an equally important role. OA evolution during a fog event is also visible from VK diagram (Fig. 7), HL and LL foggy period are split into 3 h bins from 11 pm–2 am, 2 am–5 am, 5 am–8 am as fog usually lasted from 11 pm–8 am time frame. As oxidation continues during a fog event, more oxygen containing moieties (—COOH, —CO, —C(OO)OH etc.) are being added to carbon backbone of the organic molecules leading to a decrease in H/C ratio and increase in O/C ratio. However, this kind of change is absent during non-foggy nights, indicating absence of continuous oxidation and aqueous processing. Interestingly, during both HL and LL, as fog processing continued the rate of enhancement of O/C ratio diminishes (Fig. 7) with maximum enhancement occurring from prefog to first 3 h of the fog (Fig. 7). As O/C ratio increases, fragmentation dominates over functionalization as oxidation mechanism (Kroll et al., 2009); this can lead to the escape of the highly oxidized but fragmented and more volatile organics to gas phase thus slowing down the relative enhancement of O/C ratio. Lee et al. (2012) reported similar kind of observation during laboratory oxidation of real cloud water samples. Another possible explanation for diminishing O/C ratio could be that as fog evolved from formative to mature stage, scavenging of OOAs become more efficient leading to a reduction in overall O/C ratio. These findings indicate that the combined effects of fog and OA loading can alter the OA evolution and oxidation level, but the extent of these alterations depend both on the OA loading as well as the initial background OA oxidation level.

Combined effects of fog and OA loading are also quite evident in OA composition during HL and LL period (Fig. 5). During both HL and LL foggy period, OOA mass was comparable to that of non-foggy nights and OOA contributions to total OA was higher than non-foggy nights (Fig. 5). This finding is a bit surprising as a study from Po valley (Gilardoni et al., 2014) reported higher fog scavenging efficiency for

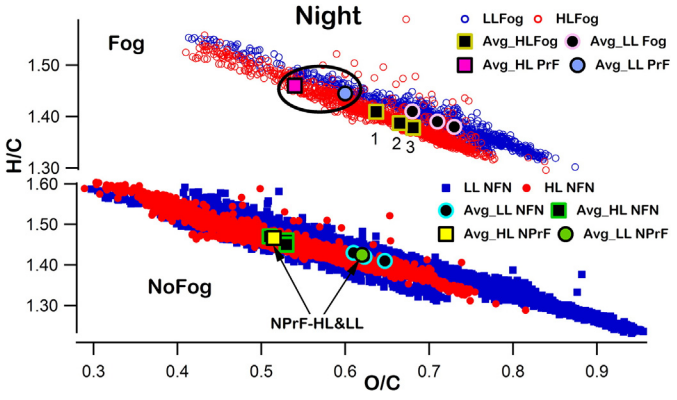

Fig. 7. Night time evolution of OA elemental ratios under fog and no foggy condition. Each big circle and squares represent the average of three equal 3 h bin from 11 pm–8 am during fog and non-foggy night. For foggy period, point 1 (black square with yellow border) represents average H/C, O/C from 11 pm–2 am of all HL fog events, point 2 for 2 am–5 am and so on, same is true for LL fog events. During foggy periods, from point 1 to 3, a continuous increase in O/C ratio and subsequent decrease in H/C ratio can be observed. However, for non-foggy period, no such systematic temporal evolution can be found, and big circles and squares from different 3 h bins are mixed. 2 points inside the black circle at the top panel are average H/C, O/C of all HL (magenta square) and LL (circular cyan) prefog period. 2 points marked by arrows in the lower panel are average H/C, O/C of all HL (yellow square) and LL (circular green) prefog period. (For interpretation of the references to colour in this figure legend, the reader is referred to the web version of this article.)

oxidized OAs. This increase OOA contribution indicates that oxidized OA was, in fact, being produced inside fog via aqueous processing as reported in some other studies (Dall'Osto et al., 2009; Kaul et al., 2011; Ge et al., 2012).

Although the trend of higher OOA contributions during fog was similar for both HL and LL period, there were some differences. During HL period, OOA contributions to total OA increased from 50% during non-foggy night to 67% during foggy period, a relative increase of 34% [{(67 − 50)/50} ∗ 100%]. During LL period, the same relative enhancement was only 16% (from 57%, during non-fogy nights to 66%, during foggy period) (Fig. 5). But during HL period, this enhancement was mainly driven by reductions in POAs rather than increase in OOAs while during LL period OOA mass concentration was increased from 41 μg/m^3 during the non-foggy night to 46 μg/m^3 during fog (Fig. 5). Fog frequency and LWC were lower (Fig. S1) during LL period, so less effective fog scavenging may have led to the higher concentration of oxidized OAs. During prefog to fog transition, absolute OOA mass was decreased by 12 μg/m^3 (98 μg/m^3 to 86 μg/m^3) and 5 μg/m^3 (51 μg/m^3 to 46 μg/m^3) for HL and LL periods, respectively. However, relative decrease was almost same for both the periods (12% and 10% for HL and LL, respectively). For POAs also, the relative reduction was almost same during both the periods (46% and 42% for HL and LL, respectively) but much higher than OOAs. This showed that fog scavenging efficiency for submicron aerosols was almost same under both loading conditions, and a reduction in POAs drove a decrease in OA loading during fog events. During both HL and LL, from fog to postfog, OOA mass was increased while no/negative changes were observed from non-foggy night to Non-post foggyday (Fig. 5).

During daytime, boundary layer (BL) expansion usually, leads to a reduction in mass concentration due to dilution. Increase in OOAs from fog (nighttime) to postfog (day time) while no change in POAs indicates (Fig. 5) OOA production via photochemistry of fog processed residuals and/or transported OOAs negated the dilution effect of BL expansion. No, or negative change in OOAs from non-foggy night to non-post foggy day indicates that dilution effect due to BL expansion was more dominant than the photochemical production and/or aerosol transport. It is also interesting to note that O-BBOA mass concentration and relative contribution to OA remain almost unchanged from fog/non-foggy night to post fog/non-post fog days while substantial changes occurred in OOA-1 and OOA-2 mass concentrations, this hints that O-BBOA was regional in nature.

4. Atmospheric implications

Results of this study indicate that depending upon OA loading, nature, type and contributions of different OOAs to OA can change drastically. This study reveals that OA loading can influence the OA composition by impacting the various types of OA differently, indicating of the highly complex nature of OA loading-oxidation relationship. Highly oxidized OA decreases most sharply whereas aged BBOA showed little dependence on OA loading. It is found that fog via aqueous chemistry could reduce the OA loading influence on OA oxidation. Influence of fog processing also varies with OA loading conditions; during HL, difference between foggy (O/C = 0.64) and non-foggy night (O/C = 0.49) O/C ratio (diff = 0.15) was much higher than the same difference during LL period (O/C = 0.70 and 0.63, respectively for foggy and non-foggy night period, diff = 0.07).

These findings indicate that under ambient conditions, only gas to particle conversion method (using OA loading dependent volatility basis set approach) based estimates of the O/C ratio can result in some underestimation of the actual O/C values. Several OA properties like volatility, hygroscopicity, and optical characteristics relate strongly to the O/C ratio. So, it is important that field and laboratory studies explore the combined influence of OA loading and aqueous processing on OA oxidation and composition for wet aerosols under high RH conditions, as seen in many regions globally. Current global SOA models should

also include loading period dependent gas to particle conversion along with heterogeneous reactions like aqueous processing to avoid erroneous estimation of degree of OA oxygenation and SOA mass concentrations.

Acknowledgments

We acknowledge the pivotal support of IIT Kanpur for providing us with an HR-ToF-AMS under PG research and teaching initiative. We acknowledge the NASA-AERONET-Solar Radiation Network team for maintaining and providing us with solar flux data for Kanpur. We would also like to acknowledge the support from the Indian Ministry of Human Resource and Development (3-21/2014-TS.1) which provide us some financial assistance to carry out this research. This research is also partially supported by the U.S. Agency for International Development (AID-OAA-A-11-00012). The data used for back trajectory analysis were obtained from the NOAA website (http://ready.arl.noaa.gov).

Appendix A. Supplementary data

Supplementary data to this article can be found online at http://dx.doi.org/10.1016/j.scitotenv.2016.08.156.

References

Aiken, A.C., DeCarlo, P.F., Jimenez, J.L., 2007. Elemental analysis of organic species with electron ionization high-resolution mass spectrometry. Anal. Chem. 79 (21), 8350–8358. http://dx.doi.org/10.1021/ac071150w.

Aiken, A.C., et al., 2008. O/C and OM/OC ratios of primary, secondary, and ambient organic aerosols with high-resolution time-of-flight aerosol mass spectrometry. Environ. Sci. Technol. 42 (12), 4478–4485. http://dx.doi.org/10.1021/es703009q.

Aiken, A.C., et al., 2010. Mexico city aerosol analysis during MILAGRO using high resolution aerosol mass spectrometry at the urban supersite (T0) - part 2: analysis of the biomass burning contribution and the non-fossil carbon fraction. Atmos. Chem. Phys. 10 (12), 5315–5341. http://dx.doi.org/10.5194/acp-10-5315-2010.

Al-Abadleh, H.a., 2015. Review of the bulk and surface chemistry of iron in atmospherically relevant systems containing humic-like substances. RSC Adv. 5 (57), 45785–45811. http://dx.doi.org/10.1039/C5RA03132J.

Allan, J.D., 2003. Correction to "Quantitative sampling using an aerodyne aerosol mass spectrometer: 1. Techniques of data interpretation and error analysis". J. Geophys. Res. Atmos. 108. http://dx.doi.org/10.1029/2003JD001607.

Bahreini, R., et al., 2009. Organic aerosol formation in urban and industrial plumes near Houston and Dallas, Texas. J. Geophys. Res. 114. http://dx.doi.org/10.1029/2008jd011493.

Bhattu, D., Tripathi, S.N., 2015. CCN closure study: effects of aerosol chemical composition and mixing state. J. Geophys. Res. Atmos. 120 (2), 766–783. http://dx.doi.org/10.1002/2014JD021978.

Brown, S.S., et al., 2009. Nocturnal isoprene oxidation over the Northeast United States in summer and its impact on reactive nitrogen partitioning and secondary organic aerosol. Atmos. Chem. Phys. 9 (9), 3027–3042. http://dx.doi.org/10.5194/acp-9-3027-2009.

Cabada, J.C., Pandis, S.N., Subramanian, R., Robinson, A.L., Polidori, A., Turpin, B., 2004. Estimating the secondary organic aerosol contribution to PM2.5 using the EC tracer method. Aerosol Sci. Technol. 38, 140–155. http://dx.doi.org/10.1080/02786820390229084.

Canagaratna, M.R., et al., 2007. Chemical and microphysical characterization of ambient aerosols with the aerodyne aerosol mass spectrometer. Mass Spectrom. Rev. 26 (2), 185–222. http://dx.doi.org/10.1002/mas.20115.

Carlton, A.G., Turpin, B.J., Altieri, K.E., Seitzinger, S., Reff, A., Lim, H.-J., Ervens, B., 2007. Atmospheric oxalic acid and SOA production from glyoxal: results of aqueous photooxidation experiments. Atmos. Environ. 41 (35), 7588–7602. http://dx.doi.org/10.1016/j.atmosenv.2007.05.035.

Chakraborty, A., Ervens, B., Gupta, T., Tripathi, S.N., 2016a. Characterization of organic residues of size-resolved fog droplets and their atmospheric implications. J. Geophys. Res. Atmos. 121 (8), 4317–4332. http://dx.doi.org/10.1002/2015JD024508.

Chakraborty, A., Gupta, T., Tripathi, S.N., 2016b. Chemical composition and characteristics of ambient aerosols and rainwater residues during Indian summer monsoon: insight from aerosol mass spectrometry. Atmos. Environ. 136, 144–155. http://dx.doi.org/10.1016/j.atmosenv.2016.04.024.

Chakraborty, A., Bhattu, D., Gupta, T., Tripathi, S.N., Canagaratna, M.R., 2015. Real-time measurements of ambient aerosols in a polluted Indian city: sources, characteristics and processing of organic aerosols during foggy and non-foggy periods. J. Geophys. Res. Atmos. 120 (17), 9006–9019. http://dx.doi.org/10.1002/2015JD023419.

Collett, J.L., Bator, A., Sherman, D.E., Moore, K.F., Hoag, K.J., Demoz, B.B., Rao, X., Reilly, J.E., 2002. The chemical composition of fogs and intercepted clouds in the United States. Atmos. Res. 64, 29–40. http://dx.doi.org/10.1016/S0169-8095(02)00077-7.

Collett, J.L., Herckes, P., Youngster, S., Lee, T., 2008. Processing of atmospheric organic matter by California radiation fogs. Atmos. Res. 87 (3–4), 232–241. http://dx.doi.org/10.1016/j.atmosres.2007.11.005.

Cubison, M.J., et al., 2011. Effects of aging on organic aerosol from open biomass burning smoke in aircraft and laboratory studies. Atmos. Chem. Phys. 11 (23), 12049–12064. http://dx.doi.org/10.5194/acp-11-12049-2011.

Dall'Osto, M., Harrison, R.M., Coe, H., Williams, P., 2009. Real-time secondary aerosol formation during a fog event in London. Atmos. Chem. Phys. 9 (7), 2459–2469. http://dx.doi.org/10.5194/acp-9-2459-2009.

De Gouw, J., Jimenez, J.L., 2009. Organic aerosols in the earth's atmosphere. Environ. Sci. Technol. 43 (20), 7614–7618. http://dx.doi.org/10.1021/es9006004.

DeCarlo, P.F., et al., 2006. Field-deployable, high-resolution, time-of-flight aerosol mass spectrometer. Anal. Chem. 78 (24), 8281–8289. http://dx.doi.org/10.1021/ac061249n.

Docherty, K.S., Jaoui, M., Corse, E., Jimenez, J.L., Offenberg, J.H., Lewandowski, M., Kleindienst, T.E., 2013. Collection efficiency of the aerosol mass spectrometer for chamber-generated secondary organic aerosols. Aerosol Sci. Technol. 47 (3), 294–309. http://dx.doi.org/10.1080/02786826.2012.752572.

Draxler, R. and Rolph, G. D. (2003), HYSPLIT (Hybrid Single-Particle Lagrangian Integrated Trajectory) Model Access Via NOAA ARL READY Website (http://www.arl.noaa.gov/ready/hysplit4.html), NOAA Air Resources Laboratory, Silver Spring, MD USA, NOAA.

Draxler, R., Stunder, B., Rolph, G., Stein, A., Taylor, A., 2014. HYSPLIT4 User's Guide. NOAA (September).

Eck, T.F., et al., 2012. Fog- and cloud-induced aerosol modification observed by the aerosol robotic network (AERONET). J. Geophys. Res. Atmos. 117 (7), 1–18. http://dx.doi.org/10.1029/2011JD016839.

Elias, T., Haeffelin, M., Drobinski, P., Gomes, L., Rangognio, J., Bergot, T., Chazette, P., Raut, J.-C., Colomb, M., 2009. Particulate contribution to extinction of visible radiation: pollution, haze, and fog. Atmos. Res. 92 (4), 443–454. http://dx.doi.org/10.1016/j.atmosres.2009.01.006.

Ervens, B., Feingold, G., Frost, G.J., Kreidenweis, S.M., 2004. A modeling study of aqueous production of dicarboxylic acids: 1. Chemical pathways and speciated organic mass production. J. Geophys. Res. 109 (D15). http://dx.doi.org/10.1029/2003jd004387.

Ervens, B., Herckes, P., Feingold, G., Lee, T., Collett, J.L., Kreidenweis, S.M., 2003. On the drop-size dependence of organic acid and formaldehyde concentrations in fog. J. Atmos. Chem. 46 (3), 239–269. http://dx.doi.org/10.1023/a:1026393805907.

Ervens, B., Sorooshian, A., Lim, Y.B., Turpin, B.J., 2014. Key parameters controlling OH-initiated formation of secondary organic aerosol in the aqueous phase (aqSOA). J. Geophys. Res. Atmos. 119 (7), 3997–4016. http://dx.doi.org/10.1002/2013JD021021.

Ervens, B., Turpin, B.J., Weber, R.J., 2011. Secondary organic aerosol formation in cloud droplets and aqueous particles (aqSOA): a review of laboratory, field and model studies. Atmos. Chem. Phys. 11 (21), 11069–11102. http://dx.doi.org/10.5194/acp-11-11069-2011.

Frank, G., et al., 1998. Droplet formation and growth in polluted fogs. Contrib. to Atmos. Phys. 71 (1), 65–85.

Ge, X., Zhang, Q., Sun, Y., Ruehl, C.R., Setyan, A., 2012. Effect of aqueous-phase processing on aerosol chemistry and size distributions in Fresno, California, during wintertime. Environ. Chem. 9 (3), 221–235. http://dx.doi.org/10.1071/en11168.

Gilardoni, S., et al., 2014. Fog scavenging of organic and inorganic aerosol in the Po Valley. Atmos. Chem. Phys. 14 (13), 6967–6981. http://dx.doi.org/10.5194/acp-14-6967-2014.

GOI, 2011. Indian Census 2011. (Website: http://www.census2011.co.in/census/district/535-kanpur-nagar.html).

Gultepe, I., et al., 2007. Fog research: a review of past achievements and future perspectives. Pure Appl. Geophys. 164, 1121–1159. http://dx.doi.org/10.1007/s00024-007-0211-x.

Gupta, T., Mandariya, A., 2013. Sources of submicron aerosol during fog-dominated wintertime at Kanpur. Environ. Sci. Pollut. Res. 20 (8), 5615–5629. http://dx.doi.org/10.1007/s11356-013-1580-6.

Gupta, A.K., Nag, S., Mukhopadhyay, U.K., 2006. Characterisation of PM10, PM2.5 and benzene soluble organic fraction of particulate matter in an urban area of Kolkata, India. Environ. Monit. Assess. 115 (1-3), 205–222. http://dx.doi.org/10.1007/s10661-006-6550-8.

Gurjar, B.R., van Aardenne, J.A., Lelieveld, J., Mohan, M., 2004. Emission estimates and trends (1990–2000) for megacity Delhi and implications. Atmos. Environ. 38 (33), 5663–5681. http://dx.doi.org/10.1016/j.atmosenv.2004.05.057.

Hallquist, M., et al., 2009. The formation, properties and impact of secondary organic aerosol: current and emerging issues. Atmos. Chem. Phys. 9 (14), 5155–5236.

Heald, C.L., Kroll, J.H., Jimenez, J.L., Docherty, K.S., Decarlo, P.F., Aiken, A.C., Chen, Q., Martin, S.T., Farmer, D.K., Artaxo, P., 2010. A simplified description of the evolution of organic aerosol composition in the atmosphere. Geophys. Res. Lett. 37 (8). http://dx.doi.org/10.1029/2010GL042737.

Jacobson, M.C., Hansson, H.C., Noone, K.J., Charlson, R.J., 2000. Organic atmospheric aerosols: review and state of the science. Rev. Geophys. 38 (2), 267–294. http://dx.doi.org/10.1029/1998rg000045.

Jimenez, J.L., et al., 2009. Evolution of organic aerosols in the atmosphere. Science 326 (5959), 1525–1529. http://dx.doi.org/10.1126/science.1180353.

Joseph, A.E., Unnikrishnan, S., Kumar, R., 2012. Chemical characterization and mass closure of fine aerosol for different land use patterns in Mumbai City. Aerosol Air Qual. Res. 12 (1), 61–72. http://dx.doi.org/10.4209/aaqr.2011.04.0049.

Kang, E., Toohey, D.W., Brune, W.H., 2011. Dependence of SOA oxidation on organic aerosol mass concentration and OH exposure: experimental PAM chamber studies. Atmos. Chem. Phys. 11 (4), 1837–1852. http://dx.doi.org/10.5194/acp-11-1837-2011.

Kaul, D.S., Gupta, T., Tripathi, S.N., 2012. Chemical and microphysical properties of the aerosol during foggy and nonfoggy episodes: a relationship between organic and inorganic content of the aerosol. Atmos. Chem. Phys. Discuss. 12 (6), 14483–14524. http://dx.doi.org/10.5194/acpd-12-14483-2012.

Kaul, D.S., Gupta, T., Tripathi, S.N., Tare, V., Collett Jr., J.L., 2011. Secondary organic aerosol: a comparison between foggy and nonfoggy days. Environ. Sci. Technol. 45 (17), 7307–7313. http://dx.doi.org/10.1021/es201081d.

Kokkola, H., Romakkaniemi, S., Laaksonen, A., 2003. On the formation of radiation fogs under heavily polluted conditions. Atmos. Chem. Phys. 3 (3), 581–589. http://dx.doi.org/10.5194/acp-3-581-2003.

Kroll, J.H., Seinfeld, J.H., 2008. Chemistry of secondary organic aerosol: formation and evolution of low-volatility organics in the atmosphere. Atmos. Environ. 42 (16), 3593–3624. http://dx.doi.org/10.1016/j.atmosenv.2008.01.003.

Kroll, J.H., Smith, J.D., Che, D.L., Kessler, S.H., Worsnop, D.R., Wilson, K.R., 2009. Measurement of fragmentation and functionalization pathways in the heterogeneous oxidation of oxidized organic aerosol. Phys. Chem. Chem. Phys. 11 (36), 8005–8014. http://dx.doi.org/10.1039/b905289e.

Kumar, A., Srivastava, D., Agrawal, M., Goel, A., 2014. Snapshot of PM loads evaluated at major road and railway intersections in an urban locality. Int. J. Environ. Prot. 4 (1), 23–29.

Lance, S., Brock, C.A., Rogers, D., Gordon, J.A., 2010. Water droplet calibration of the cloud droplet probe (CDP) and in-flight performance in liquid, ice and mixed-phase clouds during ARCPAC. Atmos. Meas. Tech. 3 (6), 1683–1706. http://dx.doi.org/10.5194/amt-3-1683-2010.

Lee, A.K.Y., Hayden, K.L., Herckes, P., Leaitch, W.R., Liggio, J., Macdonald, A.M., Abbatt, J.P.D., 2012. Characterization of aerosol and cloud water at a mountain site during WACS 2010: secondary organic aerosol formation through oxidative cloud processing. Atmos. Chem. Phys. 12 (15), 7103–7116. http://dx.doi.org/10.5194/acp-12-7103-2012.

Lee, A.K.Y., Herckes, P., Leaitch, W.R., MacDonald, A.M., Abbatt, J.P.D., 2011. Aqueous OH oxidation of ambient organic aerosol and cloud water organics: Formation of highly oxidized products. Geophys. Res. Lett. 38 (11), 1–5, L11805. http://dx.doi.org/10.1029/2011GL047439.

Lee, A.K.Y., Willis, M.D., Healy, R.M., Wang, J.M., Jeong, C.-H., Wenger, J.C., Evans, G.J., Abbatt, J.P.D., 2015. Single particle characterization of biomass burning organic aerosol (BBOA): evidence for non-uniform mixing of high molecular weight organics and potassium. Atmos. Chem. Phys. Discuss. 15 (22), 32157–32183. http://dx.doi.org/10.5194/acpd-15-32157-2015.

Li, Y.J., Lee, B.Y.L., Yu, J.Z., Ng, N.L., Chan, C.K., 2013. Evaluating the degree of oxygenation of organic aerosol during foggy and hazy days in Hong Kong using high-resolution time-of-flight aerosol mass spectrometry (HR-ToF-AMS). Atmos. Chem. Phys. 13 (17), 8739–8753. http://dx.doi.org/10.5194/acp-13-8739-2013.

Li, Z., et al., 2014. Observations of residual submicron fine aerosol particles related to cloud and fog processing during a major pollution event in Beijing. Atmos. Environ. 86, 187–192. http://dx.doi.org/10.1016/j.atmosenv.2013.12.044.

Liu, P.S.K., Deng, R., Smith, K.A., Williams, L.R., Jayne, J.T., Canagaratna, M.R., Moore, K., Onasch, T.B., Worsnop, D.R., Deshler, T., 2007. Transmission efficiency of an aerodynamic focusing lens system: comparison of model calculations and laboratory measurements for the aerodyne aerosol mass spectrometer. Aerosol Sci. Technol. 41 (8), 721–733. http://dx.doi.org/10.1080/02786820701422278.

McNeill, V.F., 2015. Aqueous organic chemistry in the atmosphere: sources and chemical processing of organic aerosols. Environ. Sci. Technol. 49 (3), 1237–1244. http://dx.doi.org/10.1021/es5043707.

Middlebrook, A.M., Bahreini, R., Jimenez, J.L., Canagaratna, M.R., 2012. Evaluation of composition-dependent collection efficiencies for the aerodyne aerosol mass spectrometer using field data. Aerosol Sci. Technol. 46 (3), 258–271. http://dx.doi.org/10.1080/02786826.2011.620041.

National Ambient Air Quality Standards, 2012. National Ambient Air Quality Status & Trends in India-2010 Central Pollution Control Board, GOI (January).

Ng, N.L., Canagaratna, M.R., Jimenez, J.L., Chhabra, P.S., Seinfeld, J.H., Worsnop, D.R., 2011a. Changes in organic aerosol composition with aging inferred from aerosol mass spectra. Atmos. Chem. Phys. 11 (13), 6465–6474. http://dx.doi.org/10.5194/acp-11-6465-2011.

Ng, N.L., Canagaratna, M.R., Jimenez, J.L., Zhang, Q., Ulbrich, I.M., Worsnop, D.R., 2011b. Real-time methods for estimating organic component mass concentrations from aerosol mass spectrometer data. Environ. Sci. Technol. 45 (3), 910–916. http://dx.doi.org/10.1021/es102951k.

Ortega, A.M., Day, D.A., Cubison, M.J., Brune, W.H., Bon, D., de Gouw, J.A., Jimenez, J.L., 2013. Secondary organic aerosol formation and primary organic aerosol oxidation from biomass-burning smoke in a flow reactor during FLAME-3. Atmos. Chem. Phys. 13 (22), 11551–11571. http://dx.doi.org/10.5194/acp-13-11551-2013.

Paatero, P., Tapper, U., 1994. Positive matrix factorization — a nonnegative factor model with optimal utilization of error estimates of data values. Environmetrics 5, 111–126. http://dx.doi.org/10.1002/env.3170050203.

Pankow, J.F., 1994. An absorption model of the gas/aerosol partitioning involved in the formation of secondary organic aerosol. Atmos. Environ. 28 (2), 189–193. http://dx.doi.org/10.1016/1352-2310(94)90094-9.

Pfaffenberger, L., Barmet, P., Slowik, J.G., Praplan, A.P., Dommen, J., Prévôt, A.S.H., Baltensperger, U., 2013. The link between organic aerosol mass loading and degree of oxygenation: an α-pinene photooxidation study. Atmos. Chem. Phys. 13 (13), 6493–6506. http://dx.doi.org/10.5194/acp-13-6493-2013.

Quan, J., Zhang, Q., He, H., Liu, J., Huang, M., Jin, H., 2011. Analysis of the formation of fog and haze in North China Plain (NCP). Atmos. Chem. Phys. 11 (15), 8205–8214. http://dx.doi.org/10.5194/acp-11-8205-2011.

Ram, K., Sarin, M.M., 2011. Day-night variability of EC, OC, WSOC and inorganic ions in urban environment of Indo-Gangetic Plain: implications to secondary aerosol formation. Atmos. Environ. 45 (2), 460–468. http://dx.doi.org/10.1016/j.atmosenv.2010.09.055.

Saarikoski, S.K., Sillanpaeae, M.K., Saarnio, K.M., Hillamo, R.E., Pennanen, A.S., Salonen, R.O., 2008. Impact of biomass combustion on urban fine particulate matter in Central and Northern Europe. Water Air Soil Pollut. 191 (1–4), 265–277. http://dx.doi.org/10.1007/s11270-008-9623-1.

Sarkar, S., Khillare, P.S., Jyethi, D.S., Hasan, A., Parween, M., 2010. Chemical speciation of respirable suspended particulate matter during a major firework festival in India. J. Hazard. Mater. 184 (1–3), 321–330. http://dx.doi.org/10.1016/j.jhazmat.2010.08.039.

Seinfeld, J.H., Pankow, J.F., 2003. Organic atmospheric particulate material. Annu. Rev. Phys. Chem. 54, 121–140. http://dx.doi.org/10.1146/annurev.physchem.54.011002.103756.

Singh, V.P., Gupta, T., Tripathi, S.N., Jariwala, C., Das, U., 2011. Experimental study of the effects of environmental and fog condensation nuclei parameters on the rate of fog formation and dissipation using a new laboratory scale fog generation facility. Aerosol Air Qual. Res. 11 (2), 140–154. http://dx.doi.org/10.4209/aaqr.2010.08.0071.

Singh, D.K., Lakshay, Gupta, T., 2014. Field performance evaluation during fog-dominated wintertime of a newly developed denuder-equipped PM1 sampler. Environ. Sci. Pollut. Res. 21 (6), 4551–4564. http://dx.doi.org/10.1007/s11356-013-2371-9.

Syed, F.S., Körnich, H., Tjernström, M., 2012. On the fog variability over south Asia. Clim. Dyn. 39 (12), 2993–3005. http://dx.doi.org/10.1007/s00382-012-1414-0.

Takegawa, N., Miyakawa, T., Kondo, Y., Jimenez, J.L., Zhang, Q., Worsnop, D.R., Fukuda, M., 2006b. Seasonal and diurnal variations of submicron organic aerosol in Tokyo observed using the aerodyne aerosol mass spectrometer. J. Geophys. Res. 111 (D11). http://dx.doi.org/10.1029/2005jd006515.

Takegawa, N., et al., 2006a. Evolution of submicron organic aerosol in polluted air exported from Tokyo. Geophys. Res. Lett. 33 (15). http://dx.doi.org/10.1029/2006gl025815.

Timonen, H., et al., 2013. Characteristics, sources and water-solubility of ambient submicron organic aerosol in springtime in Helsinki, Finland. J. Aerosol Sci. 56, 61–77. http://dx.doi.org/10.1016/j.jaerosci.2012.06.005.

Ulbrich, I.M., Canagaratna, M.R., Zhang, Q., Worsnop, D.R., Jimenez, J.L., 2009. Interpretation of organic components from positive matrix factorization of aerosol mass spectrometric data. Atmos. Chem. Phys. 9 (9), 2891–2918.

Vautard, R., Yiou, P., van Oldenborgh, G.J., 2009. Decline of fog, mist and haze in Europe over the past 30 years. Nat. Geosci. 2 (2), 115–119. http://dx.doi.org/10.1038/ngeo414.

Venkataraman, C., Reddy, C.K., Josson, S., Reddy, M.S., 2002. Aerosol size and chemical characteristics at Mumbai, India, during the INDOEX-IFP (1999). Atmos. Environ. 36 (12), 1979–1991. http://dx.doi.org/10.1016/s1352-2310(02)00167-x.

Volkamer, R., Ziemann, P.J., Molina, M.J., 2009. Secondary organic aerosol formation from acetylene (C_2H_2): seed effect on SOA yields due to organic photochemistry in the aerosol aqueous phase. Atmos. Chem. Phys. 9 (6), 1907–1928.

WMO, 1996. Guide to Meteorological Instruments and Methods of Observation. 1–2 (6), 1.8-1–1.9-1.

Yasmeen, F., Sauret, N., Gal, J.F., Maria, P.C., Massi, L., Maenhaut, W., Claeys, M., 2010. Characterization of oligomers from methylglyoxal under dark conditions: a pathway to produce secondary organic aerosol through cloud processing during nighttime. Atmos. Chem. Phys. 10 (8), 3803–3812.

Zhang, Q., Alfarra, M.R., Worsnop, D.R., Allan, J.D., Coe, H., Canagaratna, M.R., Jimenez, J.L., 2005a. Deconvolution and quantification of hydrocarbon-like and oxygenated organic aerosols based on aerosol mass spectrometry. Environ. Sci. Technol. 39 (13), 4938–4952. http://dx.doi.org/10.1021/es048568l.

Zhang, Q., Canagaratna, M.R., Jayne, J.T., Worsnop, D.R., Jimenez, J.L., 2005c. Time- and size-resolved chemical composition of submicron particles in Pittsburgh: Implications for aerosol sources and processes. J. Geophys. Res. 110 (D7). http://dx.doi.org/10.1029/2004jd004649.

Zhang, Q., Worsnop, D.R., Canagaratna, M.R., Jimenez, J.L., 2005b. Hydrocarbon-like and oxygenated organic aerosols in Pittsburgh: insights into sources and processes of organic aerosols. Atmos. Chem. Phys. 5, 3289–3311.

Zhang, Y.W., Zhang, X.Y., Zhang, Y.M., Shen, X.J., Sun, J.Y., Ma, Q.L., Yu, X.M., Zhu, J.L., Zhang, L., Che, H.C., 2015. Significant concentration changes of chemical components of PM1 in the Yangtze River Delta area of China and the implications for the formation mechanism of heavy haze–fog pollution. Sci. Total Environ. 538, 7–15. http://dx.doi.org/10.1016/j.scitotenv.2015.06.104.